IOPscience iopscience.iop.org

Home Search Collections Journals About Contact us My IOPscience

Observation of the anisotropic hopping conductivity of p-CdSb in a magnetic field

This article has been downloaded from IOPscience. Please scroll down to see the full text article.

2004 J. Phys.: Condens. Matter 16 333

(http://iopscience.iop.org/0953-8984/16/3/013)

View the table of contents for this issue, or go to the journal homepage for more

Download details:
IP Address: 129.252.86.83
The article was downloaded on 28/05/2010 at 07:49

Please note that terms and conditions apply.

INSTITUTE OF PHYSICS PUBLISHING JOURNAL OF PHYSICS: CONDENSED MATTER
J. Phys.: Condens. Matter **16** (2004) 333–342 PII: S0953-8984(04)70067-3

Observation of the anisotropic hopping conductivity of p-CdSb in a magnetic field

R Laiho[2], A V Lashkul[1], K G Lisunov[1,2,3], E Lähderanta[1,2], M O Safonchik[2,4] and M A Shakhov[1,2,4]

[1] Physics, University of Vaasa, PO Box 700, FIN-65101 Vaasa, Finland
[2] Wihuri Physical Laboratory, University of Turku, FIN-20014 Turku, Finland
[3] Institute of Applied Physics, Academiei Street 5, MD-2028 Kishinev, Moldova
[4] A F Ioffe Physico-Technical Institute, 194021 St Petersburg, Russia

Received 9 October 2003
Published 9 January 2004
Online at stacks.iop.org/JPhysCM/16/333 (DOI: 10.1088/0953-8984/16/3/013)

Abstract
The resistivity of the anisotropic semiconductor p-CdSb is investigated in a wide temperature range of $T = 1.9$–300 K in pulsed magnetic fields up to $B = 25$ T. Two not intentionally doped single-crystalline samples oriented along the crystallographic axes [100] (no. 1) and [010] (no. 2) are used for measurements of the resistivity, ρ, in transversal magnetic field configuration. Below $T \approx 8$ K the resistivity follows the laws $\ln \rho \sim CB^2$ for $B < B_c$ and $\ln \rho \sim SB^{7/12}$ for $B > B_c$, where the coefficients C and S do not depend on T, and $B_c \approx 5$–7.5 T. These are characteristics of nearest-neighbour hopping conductivity. The coefficients C and S depend on the direction of B, and their ratios agree completely with the values calculated with the components of the hole effective mass. The acceptor concentrations, $N_1 \approx 4.3 \times 10^{16}$ cm^{-3} and $N_2 \approx 7.6 \times 10^{16}$ cm^{-3} for no. 1 and no. 2, respectively, are relatively close to the critical value of the metal–insulator transition (MIT), $N_c \approx 1.2 \times 10^{17}$ cm^{-3}. This leads to enhancement of the mean localization radii, $a_1^* \approx 78$ Å in no. 1 and $a_2^* \approx 126$ Å in no. 2, with respect to the value of $a_0^* \approx 50$ Å far from the MIT determined by an asymptote of the wavefunction at a large distance from the impurity centre.

(Some figures in this article are in colour only in the electronic version)

1. Introduction

Cadmium antimonide (CdSb) is a II–V group semiconductor with orthorhombic crystal structure and an energy gap of ~0.56 eV at 0 K [1, 2]. Interest in this compound is connected to its strongly anisotropic transport properties [1–4], making designing of devices such as anisotropic thermoelectric sensors possible [5].

Not intentionally doped (in short, undoped) CdSb is a p-type semiconductor with non-degenerate charge carriers and activated conductivity [1, 2]. Its transport properties in weak magnetic fields of $B < 2$–3 T are different along the crystallographic directions **a** [100], **b** [010] and **c** [001] (signed in what follows by the subscripts 1, 2 and 3, respectively) [1, 2, 6, 7]. In undoped CdSb the resistivity, $\rho(T)$, and the Hall coefficient, $R(T)$, are determined in a wide temperature range by the activation of holes from acceptor levels at $E_1 = 6.1$ meV and $E_2 = 3.2$ meV to the valence band and by band-like conductivity over the shallow acceptor states with energies around E_2 [8]. The nature of the acceptor centres in the undoped material is connected with intrinsic defects, presumably Cd vacancies [1, 2]. Somewhat smaller values of $E_1 \approx 2.8$–4.5 meV and $E_2 \approx 1.8$–2.2 meV are found in CdSb lightly doped with Sm and Eu [9]. The shallow acceptor levels with the energies between $\sim$1 and 5 meV are obtained in CdSb doped with the elements of the I (Cu, Li, Au), II (Zn) and IV (Sn, Ge) groups (see [1, 2] and references therein).

Doping of CdSb with Ag induces a metal–insulator transition (MIT) removing the energy difference between the shallow acceptor impurity states and the valence band. This leads to the appearance of a degenerate hole gas, transforming the nature of the low-temperature conductivity from activated to metallic [2, 10]. This allows observation of the Shubnikov–de Haas effect in p-CdSb, yielding accurate values of the effective mass of the carriers. The components of the effective mass of the holes, m_i, demonstrate a weak dependence on the Hall concentration, n_R, due to non-parabolicity of the valence band. For the lowest concentration of $n_R = 1.9 \times 10^{17}$ cm^{-3}, the values of $m_i = 0.16$, 0.35 and 0.14 (in units of the free electron mass, m_0) for $i = 1$, 2 and 3, respectively, have been reported [11] and used for explicit numerical interpretation of the anisotropy of the negative magnetoresistance in p-CdSb on the *metallic* side of the MIT [12, 13].

On the *insulating* side of the MIT, the hopping conductivity of p-CdSb is expected to be anisotropic, too. However, the information about hopping charge transfer in this material is lacking, excluding an estimate of the mean localization radius of the holes $\sim$100–170 Å in CdSb lightly doped with rare-earth elements [9]. In this work we investigate the low-temperature magnetoresistance and the anisotropy of the hopping conductivity in undoped cadmium antimonide. Special emphasis is given to the magnetic field dependence of these effects.

2. Experimental results

Undoped single crystals of CdSb were grown by the zone melting technique (for details see [1, 2]). To increase the concentration of acceptors (Cd vacancies), a strong shift of the conditions of crystal growth towards the non-equilibrium state was achieved by increasing the speed of the melting zone. Generally, the initial characterization and selection of the samples can be made with measurements of the Hall effect. However, the interpretation of the temperature dependence of R in p-CdSb is a non-trivial problem due to the presence of different kinds of charge carriers, namely the holes in the two acceptor bands [8] and those activated to the various and, generally, non-equivalent extrema of the valence band [14], complicated by the anisotropy of R [7]. Therefore, Hall measurements give only approximate information about the acceptor concentration (cf the corresponding data in [6–8]), which was one of the goals of the present investigations (see below).

Two samples marked below as no. 1 and no. 2 were cut from the obtained ingot, oriented with x-ray methods, so that their short edges were parallel to the **a** and **b** directions, respectively. The measurements of $\rho(T)$ were made recording the signal from two different pairs of potential contacts in an He exchange gas dewar, where the temperature of the sample could be varied

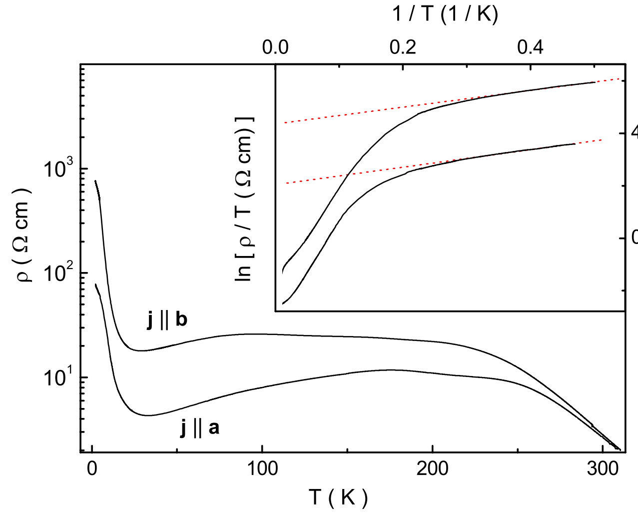

Figure 1. The temperature dependence of the resistivity of p-CdSb for no. 1 (**j** ∥ **a**) and no. 2 (**j** ∥ **b**). Inset: plots of $\ln(\rho/T)$ versus $1/T$. The dotted lines are linear fits.

between 1.9 and 300 K to an accuracy of 0.5%. Investigations of the magnetoresistance were made at a constant temperature between $T = 1.9$ and 300 K in pulsed magnetic fields B up to 25 T using the transversal field configurations of **j** ∥ **a** and **B** ∥ **b**; **j** ∥ **a** and **B** ∥ **c** (no. 1) and **j** ∥ **b** and **B** ∥ **a**; **j** ∥ **b** and **B** ∥ **c** (no. 2). The pulse length was 8 ms, and the signal from different pairs of the potential contacts was recorded with a step of 1 μs. The error in the magnetic field strength was not higher than 0.2%.

As is shown in figure 1, a pronounced difference of $\rho(T)$ is observed in the measurements of no. 1 (**j** ∥ **a**) and no. 2 (**j** ∥ **b**). In addition, the variation of $\rho(T)$ is relatively weak between 30 and 200 K but increases strongly when T is decreased below 30 K.

The dependence of ρ on B is shown in figure 2 for different configurations of the measurement. A large positive magnetoresistance (MR), increasing with the magnetic field and decreasing with increasing T, is observed. However, a small negative MR with the maximum value of $\Delta\rho/\rho \sim 1\%$ (see the inset to figure 2) is observed below $B \sim$ 1–1.5 T, decreasing rapidly when the temperature is increased. The negative MR effect disappears above $T \approx$ 3.6–4.2 K. In addition, a clear difference can be seen between the shapes of the $\rho(T)$ curves measured in no. 1 and in no. 2 (upper and lower panels of figure 2, respectively).

3. Theoretical considerations

The experimental results will be analysed using the Shklovskii and Efros theory of hopping conductivity [15] in the case of an anisotropic wavefunction of the localized charge carriers in p-CdSb. In the region of the nearest-neighbour hopping (NNH) conductivity the dependence of ρ on T is given by the expression

$$\rho(T) = \rho_0(T)\exp(\varepsilon/kT), \tag{1}$$

where the activation energy ε is independent of the temperature and the prefactor $\rho_0(T) \sim T$ [15]. Far from the MIT the value of ε does not depend on B, while the dependence of ρ_0 on B is different in the intervals of weak ($B < B_c$) and strong ($B > B_c$) magnetic fields. The weak magnetic fields shrink the impurity wavefunctions in the direction perpendicular to **B**,

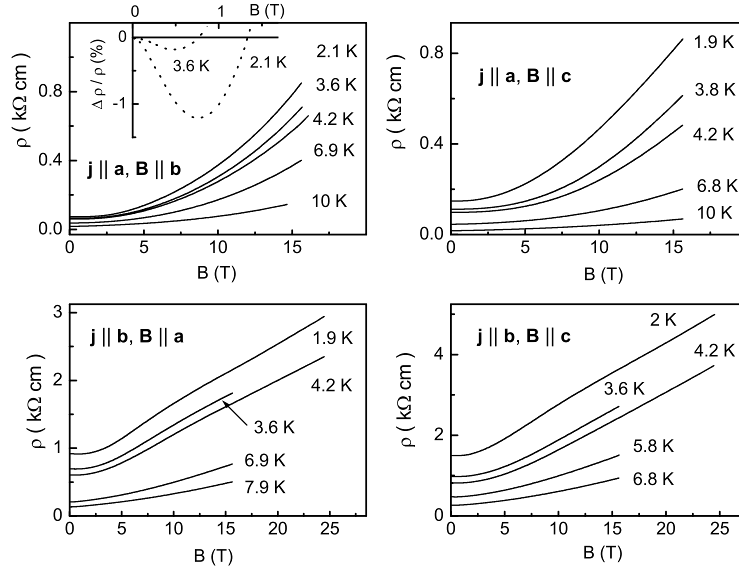

Figure 2. The dependence of the resistivity on the magnetic field in no. 1 (upper panels) and no. 2 (lower panels). Inset: the dependence of $\Delta\rho/\rho \equiv [\rho(B)-\rho(0)]/\rho(0)$ on B in the low-field region.

but do not change the energy of the impurity levels, resulting in a positive MR given by the equation

$$\ln\frac{\rho_0(B)}{\rho_0(0)} = CB^2. \tag{2}$$

Here

$$C = te^2a/(\hbar^2N), \tag{3}$$

where a is the localization radius of the charge carriers determining the space decay of the impurity wavefunction, N is the concentration of the impurities (acceptors in the case of p-CdSb) involved in the hopping charge transfer, and $t = 0.036$ [15]. In addition to shrinking of the wavefunctions, application of a strong magnetic field increases the energy of the impurity level, E, which in the case of $B_0 < B < 100B_0$ obeys the law $E(B) \approx bB^{1/3}$, where $B_0 = \hbar/(ea^2)$ is the field at which the magnetic length becomes equal to the localization radius, and b is a constant. The MR is given by the expression

$$\ln\frac{\rho_0(B)}{\rho_0'} = q\left[\frac{eB}{\hbar Na(B)}\right]^{1/2}, \tag{4}$$

where ρ_0' is a constant and $q = 0.92$ [15]. In equation (3), a does not depend on B, and far from the MIT is equal to a limiting value $a_0 = \hbar(2mE)^{-1/2}$ determined by the asymptote of the wavefunction at a large distance from the impurity centre [15] (here m is the carrier effective mass), while in equation (4), $a(B)$ far from the MIT is determined by the function $a_0(B) = \hbar[2mE(B)]^{-1/2}$. In the vicinity of the MIT the localization radius depends on N according to the scaling law

$$a(N) = a_0(1 - N/N_c)^{-\nu}, \tag{5}$$

where N_c is the critical concentration corresponding to the MIT and $\nu \approx 1$ is the critical exponent [16, 17]. The crossover of the weak and the strong fields can be estimated with the equation

$$B_c = \hbar N^{1/3}/(ea), \qquad (6)$$

where a is the localization radius in zero field. However, it has been proposed that $B_c' \approx 4B_c$ is a more accurate estimation of the crossover field than B_c [15].

The expressions above are valid for semiconductors with isotropic impurity wavefunctions. If a wavefunction is anisotropic, the MR can depend on the orientation of **B** with respect to the crystallographic axes. This dependence stems from different values of the carrier effective mass in the directions perpendicular to the magnetic field, leading to the different elasticity of the wavefunction to the magnetic shrinkage. On the other hand, the right-hand sides of equations (2) and (4) in an anisotropic semiconductor are insensitive to the direction of **j** with respect to the crystallographic axes [15].

In p-CdSb the anisotropy of the MR in the magnetic field can be found in a way almost the same as that proposed in [15] for n-Ge subjected to strong compression along the [111] direction. By a transition of the coordinate system $(x, y, z) \rightarrow (x', y', z')$, where $x = (a_1/a^*)x'$, $y = (a_2/a^*)y'$, $z = (a_3/a^*)z'$, $a_i = \hbar(2m_i E)^{-1/2}$, $i = 1, 2, 3$, and $a^* = (a_1 a_2 a_3)^{1/3}$ is the mean localization radius, the Hamiltonian of the carrier with an anisotropic effective mass in the magnetic field can be reduced to a form of a carrier with an isotropic mass $m^* = (m_1 m_2 m_3)^{1/3}$. In the vicinity of the MIT, due to equation (5), $a_i = a_{0i}(1 - N/N_c)^{-\nu}$, where $a_{0i} = \hbar(2m_i E)^{-1/2}$, $i = 1, 2, 3$, and $a^* = a_0^*(1 - N/N_c)^{-\nu}$ with $a_0^* = (a_{01} a_{02} a_{03})^{1/3}$. If the magnetic field is directed along the jth crystallographic axis, this transition conserves equations (2)–(4) but with the parameters B, m and a_0 changed to $B_j' = p_j B$, m^* and a^*, respectively, where the coefficients p_j are given by the equations

$$p_j = \left(\frac{m_j^2}{m_k m_l}\right)^{1/6}, \qquad j = 1, 2, 3; \quad j \neq k \neq l. \qquad (7)$$

Finally, the magnetic field dependence of the resistivity in p-CdSb can be conveniently expressed as

$$\ln\left[\frac{\rho_0(B)}{\rho_0(0)}\right]_{ij} = C_{ij} B^2 \qquad (8)$$

for $B < B_c$ and

$$\ln\left[\frac{\rho_0(B)}{\rho_0'}\right]_{ij} = S_{ij} B^{7/12} \qquad (9)$$

for $B > B_c$, where

$$C_{ij} = t\frac{e^2 a_0^*}{\hbar^2 N_i (1 - N_i/N_c)^{\nu}} p_j^2 \qquad (10)$$

and

$$S_{ij} = q\left[\frac{e(1 - N_i/N_c)^{\nu}}{\alpha\hbar N_i}\right]^{1/2} p_j^{7/12}. \qquad (11)$$

In equations (8)–(11), the subscripts $i = 1, 2$ and $j = 1, 2, 3$ refer to the samples (no. 1 and no. 2) and to the direction of **B** (along the jth crystallographic axis), respectively. The coefficients C_{ij} and S_{ij} are written considering the proximity to the MIT (otherwise, the case of $N_i \ll N_c$ is satisfied and the ratios N_i/N_c can be omitted). Equations (9) and (11) are obtained by taking into account the straightforward magnetic field dependence of the localization radius in a strong magnetic field (see the comments to equation (4) above), $a_0(B) \approx \alpha B^{-1/6}$ where $\alpha = \hbar(2m^* b)^{-1/2}$ is an isotropic constant.

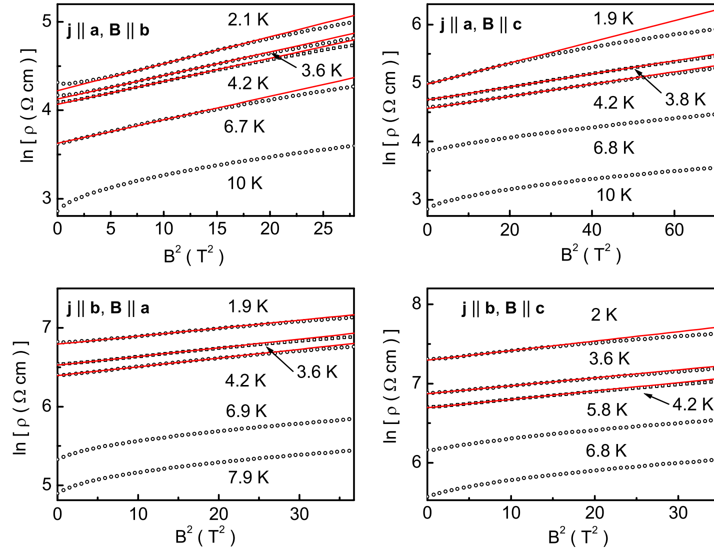

Figure 3. Plots of $\ln \rho$ versus B^2 for no. 1 (upper panel) and no. 2 (lower panel). The lines are linear fits to equation (8).

4. Analysis of the experimental data and discussion

As can be seen from the inset to figure 1, the dependences of $\ln(\rho/T)$ on $1/T$ tend to linear functions with lowering temperature. According to equation (1) this corresponds to a transition to the NNH conductivity below $T \sim 5$ K. The slopes of the plots in the inset to figure 1 give $\varepsilon \approx 0.28$ meV and 0.30 meV for no. 1 and no. 2, respectively. Therefore, the MR is analysed using equations (8)–(11).

According to equations (8) and (10) the plots of $\ln \rho$ versus B^2 in weak magnetic fields should be linear functions with the slopes independent of T. As follows from figure 3, such behaviour is realized in no. 1 between $T = 3.6$ and 4.2 K below $B \approx 4.5$ T for $\mathbf{B} \parallel \mathbf{b}$ and between $T = 3.8$ and 4.2 K below $B \approx 7.5$ T for $\mathbf{B} \parallel \mathbf{c}$ (upper panels). In no. 2 it takes place between $T = 3.6$ and 4.2 K below $B \approx 5.5$ T for $\mathbf{B} \parallel \mathbf{a}$ and below $B \approx 5.4$ T for $\mathbf{B} \parallel \mathbf{c}$ (lower panels). The deviations in low fields are connected to the onset of the negative MR, as mentioned in section 2. For $T < 3.6$–3.8 K, the plots in all panels of figure 3 can also be fitted using linear functions, due to a possible contribution from the variable-range hopping (VRH) conductivity having in low fields the same quadratic dependence of $\ln \rho$ versus T^2 but with a slope increasing with lowering temperature [15]. In turn, the deviations from linearity with increasing temperature found above 4.2 K can be interpreted by the influence of the conductivity due to thermal activation of the holes from the shallow acceptor levels to the valence band.

As follows from equations (9) and (11), in the limit of strong fields linear plots of $\ln \rho$ versus $B^{7/12}$ are expected, where the slopes should be independent of T, too. The intervals of such behaviour can be seen in figure 4, where the completion of the weak-field behaviour in figure 3 is marked by the vertical dotted lines, in no. 1 between $T = 2.1$ and 6.9 K above $B \approx 4.5$ T for $B \parallel \mathbf{b}$ (upper panels), between $T = 3.8$ and 4.2 K above $B \approx 5.8$ T for $\mathbf{B} \parallel \mathbf{c}$, and in no. 2 between $T = 7$ and 8 K above $B \approx 4.8$ T for $\mathbf{B} \parallel \mathbf{a}$ and between 4.2 and 6.8 K above $B \approx 4.9$ T for $\mathbf{B} \parallel \mathbf{c}$ (lower panels). Compared with the weak-field limit, the temperature intervals of the strong-field behaviour pertinent to the NNH conductivity are somewhat different, broadening in no. 1 (for $\mathbf{B} \parallel \mathbf{b}$) and shifting to a higher temperature in

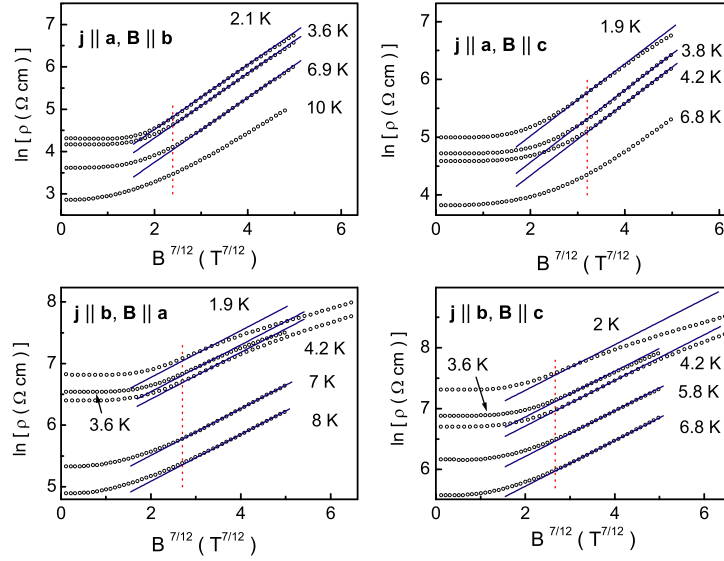

Figure 4. Plots of ln ρ versus $B^{7/12}$ for no. 1 (upper panel) and no. 2 (lower panel). The lines are linear fits of the data for **j** ∥ **a**, **B** ∥ **b** between $T = 3.6$ and 6.9 K, for **j** ∥ **a**, **B** ∥ **c** between $T = 3.8$ and 4.2 K, for **j** ∥ **b**, **B** ∥ **a** between $T = 7$ and 8 K, and for **j** ∥ **b**, **B** ∥ **c** between $T = 4.2$ and 6.8 K to equation (9). The lines falling outside the given temperature regions are drawn parallel to the linear fits for comparison. The vertical dotted line marks the upper limit of the weak-field behaviour in figure 3.

no. 2. The onset of the hopping conductivity at higher T in the strong magnetic field can be explained by increase of the energy of the shallow acceptor levels (see section 3) and damping of the contribution of the conductivity connected to the activation of the holes from the shallow acceptor levels to the valence band. On the other hand, a clear downward deviation from linearity (especially in no. 2) with lowering temperature in figure 4 suggests an enhanced contribution from the VRH conductivity in strong magnetic fields having a weaker dependence on B than the NNH conductivity [15], as will be discussed later on. Here we note that such MR behaviour cannot be attributed to the onset of the magnetic field dependence of ε in equation (1), expected in the vicinity to the MIT [15], which would lead to an upward deviation. The point is that the impurity wavefunctions are strongly overlapping near the MIT, decreasing the value of ε. A magnetic field weakens the overlapping by shrinking the wavefunctions, which can lead to an additional increase of $\rho(B)$ by increasing ε.

From the linear fits of the plots in figures 3 and 4 we obtain $C_{12} = 0.0264$, $C_{13} = 0.0108$, $C_{21} = 0.0111$, and $C_{23} = 0.0103$ (in T^{-2}), and $S_{12} = 0.765$, $S_{13} = 0.625$, $S_{21} = 0.380$ and $S_{23} = 0.375$ (in $T^{-7/12}$). For the one and the same sample (the same first subscript) the ratios between the coefficients for different directions of the field (given by the second subscript) can be expressed with equations (10) and (11) via the ratios of the corresponding components of the effective mass, $C_{ij}/C_{ik} = m_j/m_k$ and $S_{ij}/S_{ik} = (m_j/m_k)^{7/24}$. We obtain the following results: $C_{13}/C_{12} = 0.41(0.40)$, $C_{21}/C_{23} = 1.08(1.14)$, $S_{13}/S_{12} = 0.82(0.77)$, and $S_{21}/S_{23} = 1.01(1.04)$, where the values calculated with m_1, m_2 and m_3 [11] are given in parentheses. The experimental and the calculated ratios agree within a few per cent.

As mentioned above, C_{ij} and S_{ij} should not depend on the direction of **j** with respect to the crystallographic axes. From equations (10) and (11), where the subscript i refers also to the direction of **j**, it can be seen that for $N_i \ll N_c$ ($i = 1, 2$) S_{13}/S_{23} should be equal to $(C_{13}/C_{23})^{1/2}$, which is not fulfilled for our samples. Below we will show that *this is*

connected not to the sensitivity of the corresponding coefficients to the direction of the current (contradicting the theory [15]*), but to a relative proximity of the acceptor system in both samples to the MIT, where the ratios of* N_i/N_c *are not negligible and* $N_1 \neq N_2$. In this case S_{13}/S_{23} is not equal to $(C_{13}/C_{23})^{1/2}$, and the ratios between other coefficients can be expressed via these two with equations (10) and (11) as follows:

$$C_{ij}/C_{kn} = [\delta_{ik} + (1-\delta_{ik})xy]m_j/m_n \tag{12}$$

and

$$S_{ij}/S_{kn} = [\delta_{ik} + (1-\delta_{ik})(x/y)^{1/2}](m_j/m_n)^{7/24}, \tag{13}$$

where

$$x = (S_{13}/S_{23})(C_{13}/C_{23})^{1/2}, \qquad y = (S_{23}/S_{13})(C_{13}/C_{23})^{1/2}, \tag{14}$$

and δ_{ik} is the Kronecker symbol. Using the values of C_{ij} and S_{ij} obtained above we can compare the ratios of C_{ij}/C_{kn} and S_{ij}/S_{kn} for different samples ($i \neq k$) and different directions of $\mathbf{B}$($j \neq n$) with those calculated using equations (12) and (13) (in parentheses): $C_{12}/C_{21} =$ 2.38 (2.29), $C_{12}/C_{23} =$ 2.56 (2.62), $S_{12}/S_{21} =$ 2.01 (2.09), and $S_{12}/S_{23} =$ 2.04 (2.18), demonstrating an agreement within ∼2–6%.

To evaluate the values of the acceptor concentrations and the localization radii, the absolute values of the coefficients C_{12} and C_{21}, supplemented by the Mott criterion for the MIT, $N_c^{1/3}a_0^* = \beta \approx 0.25$ [16, 17], are used in the following way. Solving equation (14), where the coefficients C_{13}, C_{23}, S_{13}, and S_{23} are substituted with the right-hand sides of equations (10) and (11), we find (taking $\nu = 1$)

$$N_1 = N_c(1-y)/(x-y), \qquad N_2 = N_c x(1-y)/(x-y). \tag{15}$$

Then, substituting equations (15) and $N_c = \beta^3/(a_0^*)^3$ in equation (10), we obtain the equations for $i = 1$, $j = 2$ and $i = 2$, $j = 1$ and the respective solutions

$$a_0^* = \beta^{3/4}\left[\frac{\hbar^2}{e^2 t}\frac{(x-1)(1-y)}{(x-y)^2}\frac{C_{12}}{p_2^2}\right]^{1/4} \tag{16a}$$

and

$$a_0^* = \beta^{3/4}\left[\frac{\hbar^2}{e^2 t}\frac{xy(x-1)(1-y)}{(x-y)^2}\frac{C_{21}}{p_1^2}\right]^{1/4}. \tag{16b}$$

The values of a_0^* evaluated with equations (16*a*) and (16*b*) are found to be the same within ∼1%, yielding $a_0^* = 50$ Å. With the Mott criterion we find $N_c = 1.23 \times 10^{17}$ cm^{-3}, and with equation (15) $N_1 = 4.31 \times 10^{16}$ cm^{-3}, $N_2 = 7.55 \times 10^{16}$ cm^{-3}. Using equation (5) we get the mean localization radii of the holes, $a_1^* = 78$ Å in no. 1 and $a_2^* = 126$ Å in no. 2. Hence, it can be seen that the impurity systems in both samples are sufficiently close to the MIT to enhance the localization radii with respect to that far from the MIT, which can be calculated as $a_0^*|_{\mathrm{calc}} = \hbar/(2m^*E)^{-1/2}$ (see section 3). Using the values of $m^* = (m_1m_2m_3)^{1/3} = 0.2m_0$ and $E = E_1 = 6.1$ meV for the lower acceptor level in undoped CdSb [8], we obtain $a_0^*|_{\mathrm{calc}} = 56$ Å, in a reasonable agreement with $a_0^* = 50$ Å found in the present work.

The crossover fields evaluated with equation (6) and the relation $B_c' \approx 4B_c$ (see section 3) are $B_c = 3.0$ and 2.2 T, $B_c' = 11.9$ and 8.9 T, for no. 1 and no. 2, respectively. The values of the fields between the end of the weak-field regime and the onset of the strong-field regime are found above between ∼4.5–7.5 T and ∼4.8–5.4 T for no. 1 and no. 2, respectively, lying inside the interval of (B_c, B_c').

Finally, we discuss briefly the reason for the deviation of the plots in figure 4 from linearity with lowering temperature for no. 2 at $T \approx 2$ K, where this deviation is most pronounced. If

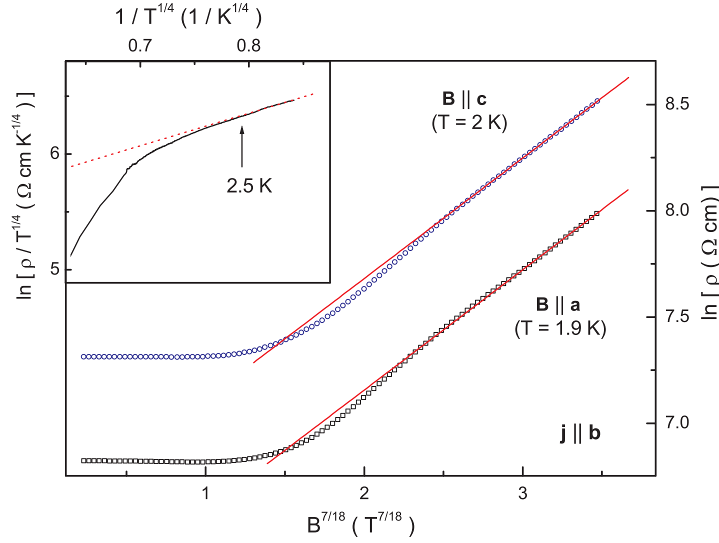

Figure 5. Plots of $\ln\rho$ versus $B^{7/18}$ in no. 2. The solid lines are linear fits. Inset: the dependence of $\ln(\rho/T^{1/4})$ on $1/T^{1/4}$, fitted with the linear function (the dotted line) below 2.5 K.

the Coulomb interaction between the carriers can be neglected, the VRH conductivity in zero field follows the Mott law [16], $\rho(T) = \rho_0(T)\exp[(T_0/T)^{1/4}]$ with $\rho_0(T) \sim T^{1/4}$, and the characteristic temperature is given by the expression $T_0 = \beta_{\rm M}/[kg(\mu)a^3]$, where $g(\mu)$ is the density of the localized states (DOS) at the Fermi level, μ, and $\beta_{\rm M} = 21$ [15]. In a strong magnetic field, taking into account the isotropic MR evaluated in [15] and the anisotropy of the acceptor states in CdSb, it can be shown in a way similar to that in section 3 for the NNH conductivity, that the prefactor obeys the law $\ln[\rho_0(B)/\rho_0']_{ij} = \chi_{ij}B^{7/18}$, where

$$\chi_{ij} = \left[\frac{\gamma e(1 - N_i/N_{\rm c})^{\nu}}{\alpha kTg(\mu)\hbar}\right]^{1/3} p_j^{7/18} \tag{17}$$

and $\gamma = 2.1$. As is evident from figure 5, the plots of $\ln\rho$ versus $B^{7/18}$ are linear above $B \sim$ 6–8 T for both directions of **B** (see figure 5), yielding $\chi_{21} = 0.567\ T^{-7/18}$, $\chi_{23} = 0.566\ T^{-7/18}$, and the ratio of $\chi_{21}/\chi_{23} = 1.002$ deviating negligibly from the value of $\chi_{21}/\chi_{23} = 1.03$ evaluated with equation (17). From equations (11) and (17) we get $g(\mu) = \gamma S_{ij}^2 N_i/(q^2\chi_{ij}^3 kT)$, giving close values of the DOS, 9.1×10^{17} meV^{-1} cm^{-3} and 8.5×10^{17} meV^{-1} cm^{-3} for $\mathbf{B} \parallel \mathbf{a}$ and $\mathbf{B} \parallel \mathbf{b}$, respectively. On the other hand, the linear fit of the plots $\ln(\rho/T^{1/4})$ versus $T^{-1/4}$ below $T \approx 2.5$ K (inset to figure 5) gives $T_0 \approx 64$ K, yielding a comparable value of $g(\mu) \approx 19 \times 10^{17}$ meV^{-1} cm^{-3}. This supports the conjecture that the downward deviation of the plots in figure 4 is caused by the transition to the VRH conductivity with lowering temperature. However, the width of the DOS $\Delta\varepsilon \approx N_2/g(\mu) \sim$ 0.1–0.2 meV seems to be too small. The point is that the Coulomb interaction of the localized carriers leads to the appearance of a parabolic gap around μ, setting in another VRH conductivity regime as predicted by Shklovskii and Efros [15]. The width of the gap can be estimated with the expression $\Delta \sim e^2/(\kappa R)$ [15], where κ is the dielectric permittivity and R is the average distance between the charge carriers. In the vicinity of the MIT, κ is scaled as $\kappa = \kappa_0(1 - N/N_{\rm c})^{-\eta}$ [16, 17], where $\eta \approx 2\nu$. With $\kappa_0 = (\kappa_1\kappa_2\kappa_3)^{1/3} \approx 25$ [18] and $N = N_2$, we obtain $\kappa \approx 160$, $R \approx 2(4\pi N_2)^{-1/3} \approx 290$ Å, and $\Delta \sim 0.3$ meV, which is comparable

with $\Delta\varepsilon$. This contradicts the supposition about non-interacting carriers in p-CdSb required for the Mott VRH conductivity.

5. Conclusions

The magnetoresistance of p-CdSb is investigated between $T = 1.9$ and 300 K in pulsed magnetic fields up to $B = 25$ T in transversal magnetic field configuration, using undoped single crystal samples oriented along the directions [100] or [010]. A dependence of the resistivity on the direction of the magnetic field with respect to the crystallographic axes is observed. The anisotropy of the resistivity in weak and strong fields is determined completely by the anisotropy of the effective mass of the holes. The nearest-neighbour hopping conductivity regime is established below $T \sim 8$ K.

Values of the acceptor concentration are relatively close to the critical concentrations of the metal–insulator transition. The average localization radii are enhanced with respect to that expected far from the metal–insulator transition, and are determined by the asymptote of the wavefunction far from the impurity centre.

Increasing deviations from the behaviour pertinent to the NNH conductivity are observed on lowering the temperature and on increasing the magnetic field and the acceptor concentration. Such behaviour is attributable to the onset of the VRH conductivity regime. Additional investigations at lower temperatures are needed before a final conclusion about the type of the VRH regime is possible.

Acknowledgments

The warm hospitality of the Wihuri Physical Laboratory, University of Turku, Finland, where the main experimental results were obtained, is gratefully acknowledged. This work was supported by the Tekniikan tutkimusinstituutti, University of Vaasa, POB 700, FIN-65101 Vaasa, Finland.

References

[1] Lazarev V B, Shevchenko V Ya, Grinberg Ya H and Sobolev V V 1978 *Semiconductor Compounds of the II–V Group* (Moscow: Nauka)
[2] Arushanov E K 1986 *Prog. Cryst. Growth Charact.* **13** 1
[3] Gelich A M and Pilat I M 2000 *Inorg. Mater.* **36** 330
[4] Semizorov A F 1998 *Inorg. Mater.* **34** 770
[5] Ashcheulov A A and Gutsul I V 2000 *J. Opt. Technol.* **67** 281
[6] Matsunami H, Nishihara Y and Tanaka T 1969 *J. Phys. Soc. Japan* **27** 1507
[7] Kawasaki T and Tanaka T 1966 *J. Phys. Soc. Japan* **21** 2475
[8] Stukan V A, Trifonov V I, Shevchenko V Ya and Goncharenko G I 1977 *Phys. Status Solidi* a **41** 307
[9] Arushanov E K, Lisunov K G, Roznovan Yu V and Shubnikov M L 1990 *Sov. Phys.—Semicond.* **24** 744
[10] Andronik I K, Arushanov E K, Emelyanenko O V and Nasledov D N 1968 *Fiz. Techn. Poluprov.* **2** 1248
[11] Arushanov E K, Cisowski J and Portal J-C 1983 *Proc. 4th All-Union Conf. on Ternary Semiconductors and their Applications* (Kishinev: Shtiintsa) p 157
[12] Arushanov E K, Lashkul A V, Lisunov K G, Parfen'ev R V and Radautsan S I 1986 *Sov. Phys.—Solid State* **28** 1334
[13] Arushanov E K, Lashkul A V, Lisunov K G, Parfen'ev R V and Radautsan S I 1987 *Sov. Phys.—Solid State* **29** 1450
[14] Tovstyuk K D, Bercha D M, Pankevich Z V and Rarenko I M 1966 *Phys. Status Solidi* **13** 207
[15] Shklovskii B I and Efros A L 1984 *Electronic Properties of Doped Semiconductors* (Berlin: Springer)
[16] Mott N F 1990 *Metal–Insulator Transitions* (London: Taylor and Francis)
[17] Castner T G 1991 *Hopping Transport in Solid* ed M Pollak and B Shklovskii (Amsterdam: Elsevier) p 3
[18] Borets A M, Rarenko I M and Rusnak V V 1984 *Proc. 6th All-Union Joint Conf. on Materials Science of II–V Semiconductor Compounds* (Moscow: IONH) p 108